555

555

Thomas

1-27-81

(1)

R-1405

SAND80-1418
Unlimited Release
UC-70

A Material Constitutive Model for Jointed Rock Mass Behavior

MASTER

Robert K. Thomas

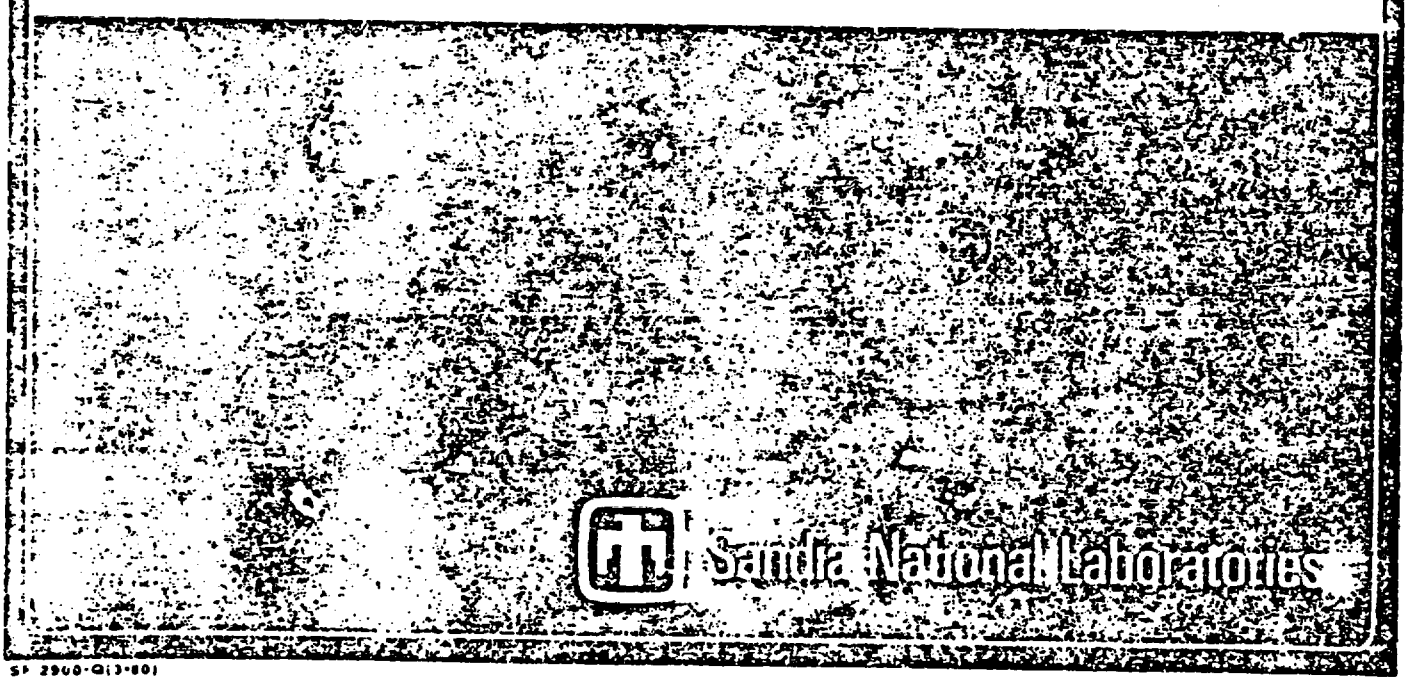

ACKNOWLEDGEMENT

The author expreses his appreciation to J. H. Biffle and R. D. Krieg, Applied Mechanics Division 5521; R. Rodeman, Applied Mechanics Division 5524; and S. W. Key, Computational Physics and Mechanics Division 5531, Sandia National Laboratories, for their considerate advice and assistance throughout the course of this study.

CONTENTS

ILLUSTRATIONS

Figure | Page

NOMENCLATURE

Symbol	Meaning
a,b	material axes
$\underset{\sim}{C}$	material stiffness tensor
C_0	cohesion
$\underset{\sim}{D}$	material compliance tensor
d	incremental operator
E	elastic modulus
$\underset{\sim}{e}$	strain tensor
G	shear modulus
g	gravitational constant
h	distance below surface of earth
i,j,k,l	indices, subscripts
k	dispersion coefficient
n, n + 1	load increments
P	cumulative probability
p	random number (0,1)
T	matrix transpose, superscript
$\underset{\sim}{t}_e$, $\underset{\sim}{t}_\sigma$	transformation matrices
x,y	global axes
$\underset{\sim}{\alpha}$	vector of thermal expansion coefficients
$\bar{\alpha}$	mean orientation of joint set
ξ	local orientation of fracture
γ	engineering shear strain
ΔT	temperature increment

Symbol	Meaning
Δ	defined in Eq. 5
η	reduction factor in Eqs. 21 and 25
μ	friction coefficient
ν	Poisson's ratio
ρ	material density
$\underset{\sim}{\sigma}$	stress tensor
σ_H, σ_V	horizontal and vertical in-situ stress components
τ	shear stress
ϕ	deviation of local fracture angle from mean direction

INTRODUCTION

The underground burial of nuclear waste has so far been proposed for both soft rock, exclusively salt, and hard rock, specifically basalt, granite, shale and tuff. This gives rise to two different geotechnical problems. The division is made because the mechanical behavior of salt is characterized by time-dependent creep deformation, while the mechanical behavior of hard rocks is generally assumed to be elastic-plastic. Additionally, salt is thought of as a continuous rock mass while hard rocks, which usually contain numerous faults and intersecting joint sets, are considered to be discontinuous. A discontinuous rock mass is described by the properties of the fractures and by the properties of the intact rock. For very hard rocks the mass behavior is controlled primarily by the discontinuities, and the behavior of the intact rock is almost irrelevant. However, for moderately hard rocks the intact rock characteristics may be dominant. In this report a material constitutive model is presented which takes explicit account of the properties of both the intact rock and the fractures. Even though immediate application is the analysis of an underground nuclear waste repository in hard rock, the constitutive model is intended to be valid for a variety of problems, both static and dynamic, in a regularly jointed medium.

Large rock masses in the earth's crust are commonly broken into block structures by fractures that occur in sets of regularly spaced, more or less parallel, planes with a variety of orientations. These joint sets are formed primarily by flow banding and cooling in igneous rocks, and by foliation in metamorphic rocks. In addition, jointing can result from up-lift of initially deep-seated rock masses. Major joint sets can extend for miles, and joint spacing can vary from centimeters to several meters. Moreover, these features can occur in lithologic units at depths of several kilometers. In this report, the words fracture and joint are used interchangeably to refer to discontinuities that have not undergone detectable shear displacement. Discontinuities that do not occur in regular sets and/or have undergone observable shear displacement are called faults or dikes. A complete description of the structural geology of joint sets is not presented here but can be found in Refs. 1-3.

The nature of the fractures observed in a hard rock mass deserves special consideration since it dictates the type of material constitutive model which must be employed for mechanical modelling. Naturally occurring fractures are found in configurations varying from the closely spaced, multiply-intersecting and omnidirectional network shown schematically in Fig. 1A, to the isolated but well-defined discrete fault illustrated in Fig. 1C. The fracture network in

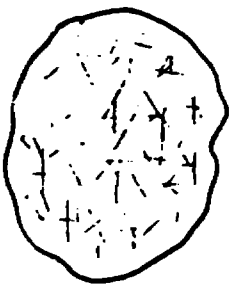

A. Multiply Jointed, Approximately Granular, Material

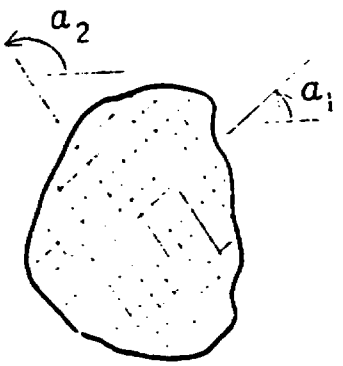

B. Regularly Jointed Rock Mass

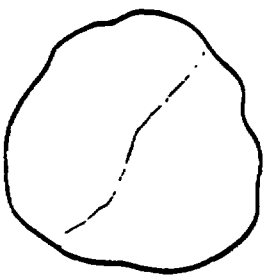

C. Discrete Fracture or Fault

Fig. 1 Classification of Hard Rock Masses for Mechanical Modelling.

Fig. 1A is typical of the Eleana shale formation at the Nevada Test Site, for which a granular materials model was found to accurately predict the rock mass response in a near surface heater experiment [4]. At the other extreme, the discrete fault in Fig. 1C is satisfactorily modelled by a slide line, with the host rock behavior being approximated by classical elastic-plastic theory. The fractures found to occur most commonly in hard rocks, however, are those depicted in Fig. 1B; they consist of one, two, or three intersecting sets, each set being defined by a typical fracture length, an average spacing between fractures, and a preferred orientation. In contrast to the granular material in Fig. 1A, the joint sets in Fig. 1B possess preferred planes of weakness. And, in contrast to the discrete fault in Fig. 1C, they are dispersed throughout the region of interest and therefore require a continuum description. It is this type of fracture system that has recently attracted special attention in the underground waste disposal community, and to which this study is addressed.

After obvious initial efforts to model fractured rock masses as homogeneous and isotropic, researchers in rock mechanics began to borrow from the established theories of soil mechanics. Generalized elastic-plastic theories with pressure-dependent yield surfaces were presented by Reyes and Deere [5] and Pariseau, Voight and Dahl [6]. Zienkiewicz [7] used a linear elastic model with a tension cutoff to

approximate the behavior of materials in which loss of cohesion occurs under tensile loading. Models for discrete joints or faults were incorporated into finite-element computer codes by Goodman, Taylor and Brekke [8] and by Ghaboussi, Wilson and Isenberg [9], and into boundary element codes by Roberds [10]. These discrete joint elements are state-of-the-art in the sense that they attempt to model nonlinear normal and shear deformation, dilatancy, and yielding with a generalized Mohr-Coulomb theory. Dixon and Mahtab [11] were among the first to report a finite element continuum model for jointed rock masses, but its applicability was limited to stability analysis; post-failure frictional slippage along pre-existing joint planes was not considered. Cundall [12] presented a theory for a continuum divided into a large number of rigid blocks where deformation takes place only between mating surfaces. Since post-failure rigid body motion could be modelled using this theory, it has been applied to earth subsidence problems. Recent advances toward a continuum theory have taken either the approach of Singh [13], Morland [14], and Zienkiewicz and Pande [15], in which fractures are modelled explicitly in the material stiffness, or the approach reported in Ref. [16] in which slip planes are modelled implicitly in the equation for the yield surface.

Geological observations and measurements in underground exploratory tunnels, of surface outcrops, and in drill holes can provide reasonably accurate information on the orientation and position of major faults. Similar field measurement data on regular joint sets, however, always exhibit scatter to some significant extent regardless of the rock type. Joint sets do not exist as perfectly parallel, planar surfaces. Their observable properties, namely spacing, size and orientation, can only be interpreted in a statistical manner. Although the major effort has been directed toward analyzing orientation data, probability distributions for joint size have been reported by Cruden [17], and for joint spacing by Snow [18] and Priest & Hudson [19]. In each case, the data were well represented by a lognormal distribution. More recently, a major effort has been undertaken to quantify several joint set characteristics for use in studies of underground nuclear waste disposal in basalt [20] and granite [21].

The assumption often made in continuum theories for regularly jointed rock masses is that fractures are everywhere planar. Zienkiewicz and Pande [15] discuss the possibility of specifying "random joints" in their finite element code, but make no attemption to relate the randomness to geologic field data. For the jointed rock model presented in this report, the fracture orientation at a point is taken as a sample from a population distribution which has been determined from field

observations. Probability distributions for joint orientation data are well established, and are presented in this report as the basis for specifying joints in the constitutive model. The assumption of parallel fracture planes is not only physically unrealistic, but may create an ill-conditioning of the global material stiffness which would contribute to the model a degree of instability that would otherwise not exist.

Fracture spacing, like fracture orientation, significantly affects rock mass behavior and must be included in the constitutive model. If the stress-strain behavior of both the intact rock and a single fracture are known individually, then constructing a constitutive relation for a composite with a given fracture spacing is straightforward. This relation is valid for finite elements with characteristic dimensions large compared to the fracture spacing. However, if the finite element dimensions are small compared to fracture spacing, then the fractures appear to be discrete and are generally modelled by slide lines or discrete joint elements. Both situations are illustrated in Fig. 2. It becomes an arduous task, both in manpower and computer time, to model a large number of discrete faults. In the present model, discrete fractures can be arbitrarily assigned at finite element integration points, and thus the continuum approximation is maintained. These elements have the normal and shear mechanical properties of an isolated joint, but adjacent elements have properties of the intact

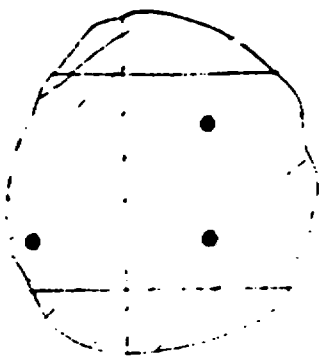

A. Fracture Spacing Small Compared To Element Size

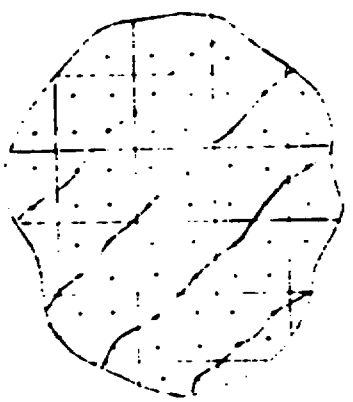

B. Fracture Spacing On The Order Of, Or Larger Than, Element Size

Fig. 2 Finite Element Models Of Joint Sets With Variable Length, Spacing And Orientation

rock. This is shown in Fig. 2B. A consistent formulation for a large range of joint spacings, with respect to finite element dimensions, has not been defined at the present time. The extension of the present model to joint sets with variable spacings based on a probability distribution, however, proceeds in the same manner as that for variable orientations which is described in this paper.

CONSTITUTIVE EQUATIONS FOR AN ELASTIC ORTHOTROPIC BODY

The constitutive equations for an elastic orthotropic body are well established and documented in the literature. They are presented here, however, because it is these equations that are modified, as shown in the next section, to model the mechanics of jointed rock masses. The equations in this section are, for the most part, taken from Johnson and Henderson [22] and Jones [23].

For a linear elastic, anisotropic material the stress-strain-temperature constitutive relationship is given by

$$\underset{\sim}{e}_{ij} = \underset{\sim}{D}_{ijkl}\, \underset{\sim}{\sigma}^{kl} + \underset{\sim}{\alpha}_{ij}\, \Delta T \ . \qquad (1)$$

Consider the two-dimensional axisymmetric or plane strain body shown in Fig. 3 with three planes of elastic symmetry (orthotropic), and where the a,b coordinates are principal material coordinates. For this case Eq. (1) reduces to

$$\begin{bmatrix} e_{aa} \\ e_{bb} \\ \gamma_{ab} \\ e_{cc} \end{bmatrix} = \begin{bmatrix} \frac{1}{E_a} & -\frac{\nu_{ba}}{E_b} & 0 & -\frac{\nu_{ca}}{E_c} \\ -\frac{\nu_{ab}}{E_a} & \frac{1}{E_b} & 0 & -\frac{\nu_{cb}}{E_c} \\ 0 & 0 & \frac{1}{G_{ab}} & 0 \\ -\frac{\nu_{ac}}{E_a} & -\frac{\nu_{bc}}{E_b} & 0 & \frac{1}{E_c} \end{bmatrix} \begin{bmatrix} \sigma_{aa} \\ \sigma_{bb} \\ \sigma_{ab} \\ \sigma_{cc} \end{bmatrix} + \Delta T \begin{bmatrix} \alpha_a \\ \alpha_b \\ 0 \\ \alpha_c \end{bmatrix} \quad (2)$$

Eq. (2) can be expressed more briefly as

$$\underset{\sim}{e}_{ab} = \underset{\sim}{D}_{ab}\, \underset{\sim}{\sigma}_{ab} + \underset{\sim}{\alpha}_{ab}\, \Delta T, \quad (3)$$

from which the stresses are given by

$$\underset{\sim}{\sigma}_{ab} = \underset{\sim}{D}_{ab}^{-1} (\underset{\sim}{e}_{ab} - \underset{\sim}{\alpha}_{ab}\, \Delta T) = \underset{\sim}{C}_{ab} (\underset{\sim}{e}_{ab} - \underset{\sim}{\alpha}_{ab}\, \Delta T). \quad (4)$$

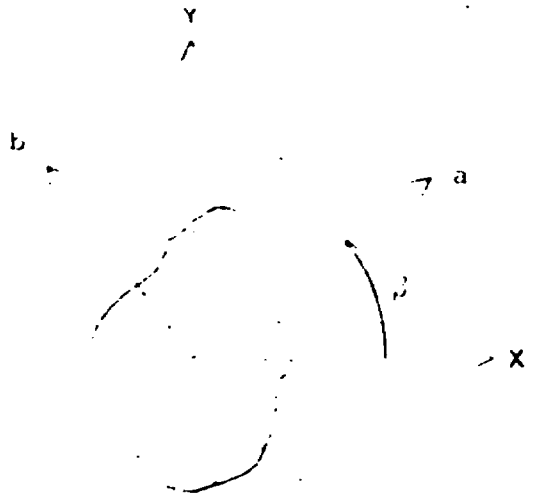

FIG. - TWO-DIMENSIONAL BODY WITH MATERIAL AXES (a,b) INCLINED TO THE GLOBAL AXES (X,Y) BY THE ANGLE β.

The non-zero components of the material stiffness $\underset{\sim}{C}_{ab}$ are

$$C_{11} = \frac{1 - \nu_{bc}\,\nu_{cb}}{E_b\,E_c\,\Delta}$$

$$C_{12} = \frac{\nu_{ba} + \nu_{ca}\,\nu_{bc}}{E_b\,E_c\,\Delta} = \frac{\nu_{ab} + \nu_{cb}\,\nu_{ac}}{E_a\,E_c\,\Delta}$$

$$C_{14} = \frac{\nu_{ca} + \nu_{ba}\,\nu_{cb}}{E_b\,E_c\,\Delta} = \frac{\nu_{ac} + \nu_{ab}\,\nu_{bc}}{E_a\,E_c\,\Delta} \qquad (5)$$

$$C_{22} = \frac{1 - \nu_{ac}\,\nu_{ca}}{E_a\,E_c\,\Delta}$$

$$C_{24} = \frac{\nu_{cb} + \nu_{ab}\,\nu_{ca}}{E_a\,E_c\,\Delta} = \frac{\nu_{bc} + \nu_{ba}\,\nu_{ac}}{E_a\,E_b\,\Delta}$$

$$C_{33} = \frac{1}{G_{ab}}$$

$$C_{44} = \frac{1 - \nu_{ab}\,\nu_{ba}}{E_a\,E_b\,\Delta} ,$$

where

$$\Delta = \frac{1 - \nu_{ab}\,\nu_{ba} - \nu_{bc}\,\nu_{cb} - \nu_{ca}\,\nu_{ac} - \nu_{ab}\,\nu_{bc}\,\nu_{ca} - \nu_{ba}\,\nu_{cb}\,\nu_{ac}}{E_a\,E_b\,E_c} .$$

If the material principal coordinates a,b do not coincide with the global coordinates x,y but are inclined by the angle β as shown in Fig. 3, then the material stiffness $\underset{\sim}{C}_{ab}$ is transformed to global coordinates by

$$\underset{\sim}{C}_{xy} = \underset{\sim}{t}_e^T\,\underset{\sim}{C}_{ab}\,\underset{\sim}{t}_c , \qquad (6)$$

where

$$\underset{\sim}{t}_e = \begin{bmatrix} \cos^2\beta & \sin^2\beta & \sin\beta\cos\beta & 0 \\ \sin^2\beta & \cos^2\beta & -\sin\beta\cos\beta & 0 \\ -2\sin\beta\cos\beta & 2\sin\beta\cos\beta & \cos^2\beta-\sin^2\beta & 0 \\ 0 & 0 & 0 & 1 \end{bmatrix} \tag{7}$$

The strains ε_{xy} in the global coordinates x,y are transformed to the material coordinates a,b by

$$\underset{\sim}{\varepsilon}_{ab} = \underset{\sim}{t}_e \, \underset{\sim}{\varepsilon}_{xy}, \tag{8}$$

and the stresses σ_{xy} are transformed by

$$\underset{\sim}{\sigma}_{ab} = \underset{\sim}{t}_\sigma \, \underset{\sim}{\sigma}_{xy}. \tag{9}$$

The transformation matrix $\underset{\sim}{t}_\sigma$ is

$$\underset{\sim}{t}_\sigma = \begin{bmatrix} \cos^2\beta & \sin^2\beta & 2\sin\beta\cos\beta & 0 \\ \sin^2\beta & \cos^2\beta & -2\sin\beta\cos\beta & 0 \\ -\sin\beta\cos\beta & \sin\beta\cos\beta & \cos^2\beta-\sin^2\beta & 0 \\ 0 & 0 & 0 & 1 \end{bmatrix} \tag{10}$$

The difference between Eqs. (7) and (10) is due to the usage here of the engineering shear-strain measure γ. The inverse transformations are given by

$$\underset{\sim}{e}_{xy} = \underset{\sim}{t}_e^{-1}\, \underset{\sim}{e}_{ab} = \underset{\sim}{t}_e(-\bar{\theta})\, \underset{\sim}{e}_{ab}$$

$$\underset{\sim}{\varepsilon}_{xy} = \underset{\sim}{t}_\varepsilon^{-1}\, \underset{\sim}{\varepsilon}_{ab} = \underset{\sim}{t}_\varepsilon(-\bar{\theta})\, \underset{\sim}{\varepsilon}_{ab} \qquad (11)$$

and

$$\underset{\sim}{\alpha}_{xy} = \underset{\sim}{t}_\varepsilon^{-1}\, \underset{\sim}{\alpha}_{ab} \,.$$

The elements of the material stiffness C_{ab} and the thermal expansion coefficients α_{ab} are considered to be temperature dependent.

MODIFICATION OF ELASTIC CONSTITUTIVE EQUATIONS TO MODEL JOINT BEHAVIOR

In the last section stress-strain relations were presented for an elastic orthotropic body. Consider now a jointed rock mass with one or more families of parallel planes of weakness. The stress-strain behavior at a point is approximately transversely isotropic, and can therefore be derived from the orthotropic equations, with major nonlinearities introduced for displacements normal and parallel to the fracture surface.

During execution of static finite element codes, calls are made to a material constitutive subroutine to obtain the stresses. In general, the stresses $\underset{\sim}{\sigma}^n_{xy}$ and strains $\underset{\sim}{e}^n_{xy}$ at the

end of the $n^{\underline{th}}$ load step are known, as are the current, or $n+1^{\underline{st}}$ strain increments, $\underset{\sim}{de}_{xy}^{n+1}$. It is required to calculate the stresses, $\underset{\sim}{\sigma}_{xy}^{n+1}$, at the end of the load step under consideration. If a predictor-corrector iteration procedure is used within a load step to account for nonlinearities, then the current value of the tangent stiffness $\underset{\sim}{C}_{xy}^{n+1}$, is also required. For the constitutive model presented here, the elastic material stiffness given by Eqs. (4) and (5) is evaluated at each load step and then modified, depending upon the joint behavior, to obtain the tangent stiffness. By proceeding in this manner, the material stiffnesses need not be stored in a working array.

If a joint is present at a finite element integration point, then the stress-strain behavior at this point is assumed to be as shown in Fig. 4 . Consider a jointed surface inclined by the angle β with respect to the global x,y coordinate axes. First, the incremental strains $\underset{\sim}{de}_{xy}^{n+1}$ are transformed to the local joint coordinate system a,b by Eq. (8). Likewise, the stresses $\underset{\sim}{\sigma}_{xy}^{n}$ that prevail at the end of the previous load step are transformed to the a, b coordinate system using Eq. (9), and the elastic material stiffness $\underset{\sim}{C}_{xy}$ is transformed using Eq. (6). An elastic incremental trial stress is then calculated using the equation,

$$d\underset{\sim}{\sigma}_{ab}^{n+1} = \underset{\sim}{C}_{ab}\, d\underset{\sim}{\epsilon}_{ab}^{n+1}, \qquad (12)$$

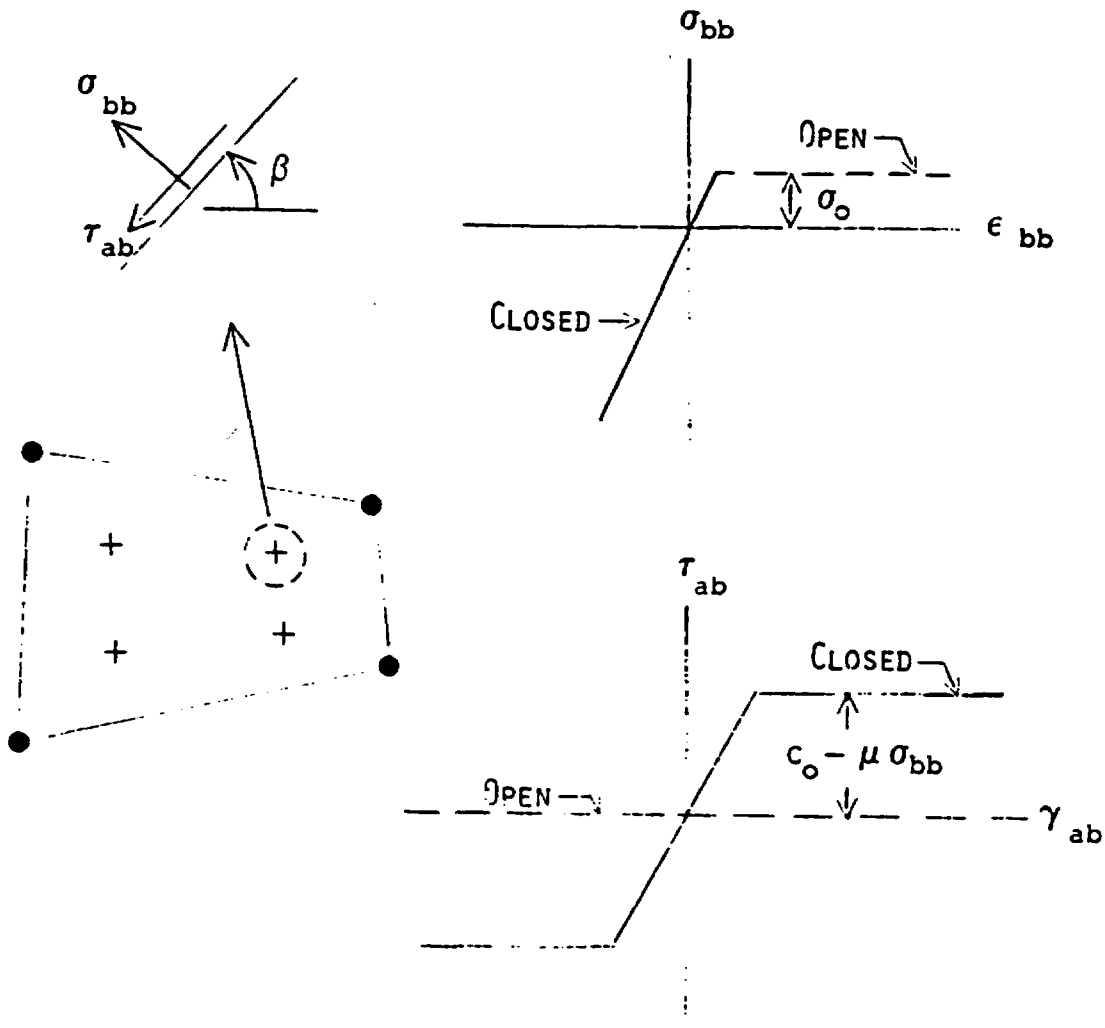

FIG. 4 JOINTED ROCK MASS BEHAVIOR IN CONSTITUTIVE MODEL

and the updated total stress is found by adding this increment to the previous value of the stress,

$$\underset{\sim}{\sigma}_{ab}^{n+1} = \underset{\sim}{\sigma}_{ab}^{n} + d\underset{\sim}{\sigma}_{ab}^{n+1} . \tag{13}$$

Joint behavior is such that tensile stresses cannot develop on planes normal to the joint surface, yet joints have full memory of any transverse displacement occurring during their excursions into the tensile zone and are able to transmit compressive stresses in the normal direction upon subsequent closure of the joint.

The strain e_{bb}^{n+1} normal to the joint plane measures joint opening and closing. This quantity is updated at each load step using the formula,

$$e_{bb}^{n+1} = e_{bb}^{n} + de_{bb}^{n+1} , \tag{14}$$

and the result is stored in a working array for subsequent retrieval.

If $e_{bb}^{n+1} > 0$ the joint is considered to be open, and both the normal stress and the shear stress on the free surface are set to zero in the updated stress array of Eq. (13),

$$\sigma_{bb}^{n+1} = \tau_{ab}^{n+1} \equiv 0. \tag{15}$$

Modifications to the elastic material stiffness to obtain the tangent stiffness must reflect a zero normal stress and thus produce a state of plane stress in the layer of material bounding the joint. If the incremental stress-strain relationship of Eq. (12) is written in the form

$$d\begin{Bmatrix}\sigma_{aa}\\ \sigma_{bb}\\ \tau_{ab}\\ \sigma_{cc}\end{Bmatrix}^{n+1} = \begin{bmatrix} C_{11} & C_{12} & 0 & C_{14}\\ C_{21} & C_{22} & 0 & C_{24}\\ 0 & 0 & C_{33} & 0\\ C_{41} & C_{42} & 0 & C_{44}\end{bmatrix} d\begin{Bmatrix}e_{aa}\\ e_{bb}\\ \alpha_{ab}\\ e_{cc}\end{Bmatrix}^{n+1} , \tag{16}$$

it follows that

$$d\sigma_{bb}^{n+1} = C_{21}\, de_{aa}^{n+1} + C_{22}\, de_{bb}^{n+1} + C_{24}\, de_{cc}^{n+1} = 0. \tag{17}$$

Solving this equation for the incremental normal strain,

$$de_{bb}^{n+1} = -\frac{C_{21}}{C_{22}}\, de_{aa}^{n+1} - \frac{C_{24}}{C_{22}}\, de_{cc}^{n+1} , \tag{18}$$

and substituting this result into Eq. (16), yields the stiffness with a vanishing normal stress,

$$\underset{\sim}{C}_{ab} = \begin{bmatrix} C_{11} - \frac{C_{12}\,C_{21}}{C_{22}} & 0 & 0 & C_{14} - \frac{C_{12}\,C_{24}}{C_{22}} \\ 0 & 0 & 0 & 0 \\ 0 & 0 & C_{33} & 0 \\ C_{41} - \frac{C_{42}\,C_{21}}{C_{22}} & 0 & 0 & C_{44} - \frac{C_{42}\,C_{24}}{C_{22}} \end{bmatrix} \tag{19}$$

To complete the description for an open joint, the additional constraint equation

$$C_{33} = 0 \quad , \tag{20}$$

is required for a zero stiffness in shear. In practice no diagonal element of the material stiffness matrix can be zero, since this leads to singular equations. The technique employed here is to multiply appropriate elements of the matrix by a positive factor η where $\eta << 1$. In this manner we obtain

$$\underset{\sim}{C}_{ab} = \begin{bmatrix} C_{11} - \dfrac{C_{12}\,C_{21}}{C_{22}} & \eta\, C_{12} & 0 & C_{14} - \dfrac{C_{12}\,C_{24}}{C_{22}} \\ \eta\, C_{21} & \eta\, C_{22} & 0 & \eta\, C_{24} \\ 0 & 0 & \eta\, C_{33} & 0 \\ C_{41} - \dfrac{C_{42}\,C_{21}}{C_{22}} & \eta\, C_{42} & 0 & C_{44} - \dfrac{C_{42}\,C_{24}}{C_{22}} \end{bmatrix} \tag{21}$$

for the final form of the tangent stiffness at a joint. The last step is to transform the stiffness and the updated stress array back to global coordinates x,y.

If $e_{bb}^{n+1} < 0$ then the joint is considered to be closed. The stress strain equations in this case are elastic unless frictional slippage occurs along the prescribed joint planes. In this study, the onset of frictional slippage is dictated by the two-dimensional Mohr-Coulomb failure surface shown in Fig. 5. The linear form is defined by the cohesion C_o, and the friction coefficient $\tan\phi$, both of which are obtained from laboratory test data.

When the joint is closed, the numerical procedure consists of determining whether or not frictional slippage is taking place, and if so, to reduce the material stiffness for shear deformation. The initial step is to make the transformations

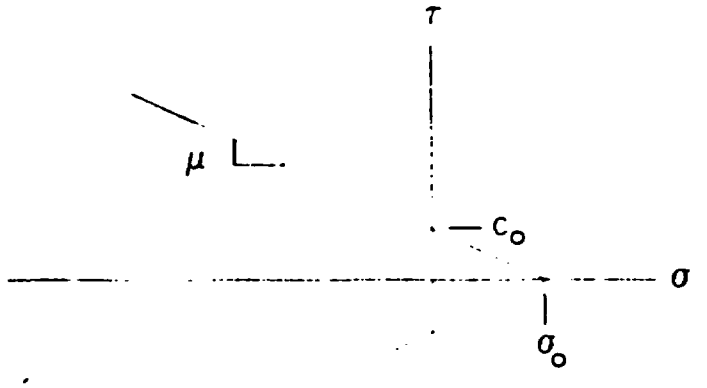

FIG. 5 LINEAR MOHR-COULOMB FAILURE SURFACE GIVEN BY $|\tau| = c_o - \mu\sigma$

to local joint axes a,b and to obtain an elastic trial stress in the same manner as previously described for the open joint. If

$$\left|\tau_{ab}^{n+1}\right| < C_o + \mu\sigma_{bb}^{n+1} \quad , \tag{22}$$

then slippage is not impending, and the elastic shear stiffness is correct. However, if

$$\left|\tau_{ab}^{n+1}\right| \geq C_o + \mu\sigma_{bb}^{n+1} \quad , \tag{23}$$

then slippage has occurred. In the updated stress array of Eq. (13) we set

$$\tau_{ab}^{n+1} = C_0 + \mu\sigma_{bb}^{n+1} \quad . \tag{24}$$

The tangent stiffness is taken to be

$$\underset{\sim}{C}_{ab} = \begin{bmatrix} C_{11} & C_{12} & 0 & C_{14} \\ C_{21} & C_{22} & 0 & C_{24} \\ 0 & 0 & \eta C_{33} & 0 \\ C_{41} & C_{42} & 0 & C_{44} \end{bmatrix} \tag{25}$$

where, as before, η is a positive factor such that $\eta \leq 1$. Finally, all arrays are transformed back to the global x,y coordinate system.

It can be seen that if two joint planes are prescribed at a finite element integration point, then the above procedure is simply repeated using the second joint angle. The factor η in Eqs. (21) and (25) can significantly influence the calculated results, and in some cases lead to undesirable results if not properly assigned. A limited amount of information is available on finite element codes with similar constitutive models [22, 24, 25, 26], and it shows that sufficiently accurate results can be obtained if η is of the order 10^{-4} to 10^{-3}. Values smaller than this do not improve the accuracy and may lead to numerical instability, while values larger than this may not reproduce the desired stresses at a joint.

STATISTICS OF JOINT ORIENTATION DATA

Geological field data on joint orientations can be presented as points mapped onto a sterographic projection. Although it is beyond the scope of this report to present a thorough description of the properties and techniques of sterographic projections, a brief summary of basic construction principles is presented here. More information can be found in Goodman [1].

Stereographic projection is a method of mapping the surface of a sphere onto a plane. As illustrated in Fig. 6, the normal direction to a joint plane is indicated by a point on the upper hemisphere of a reference sphere. Any point on the surface of the sphere is projected onto a diametral plane of the sphere (the projection plane) by means of construction lines radiating from a focus point, which is generally fixed at the lower pole position on a line perpendicular to the projection plane. Nearly vertical fracture planes therefore map as points close to the perimeter of the projection plane, while horizontal fracture planes map as points near the center of the projection plane.

The present established method of describing joint orientations based on field data is to (1) identify clusters or groupings on the stereographic projection which compose a joint set, (2) calculate the mean or average orientation of the fractures within each cluster, and (3) calculate the distribution of deviations from the mean within each cluster. The field data are almost always plotted in an equal-area stereonet which is amenable to statistical treatment. The statistics employed to model the orientation field data are based on the pioneering work of Arnold [27], Fisher [28], Watson [29], and others on the application of spherical probability distributions to geologic observations. Early

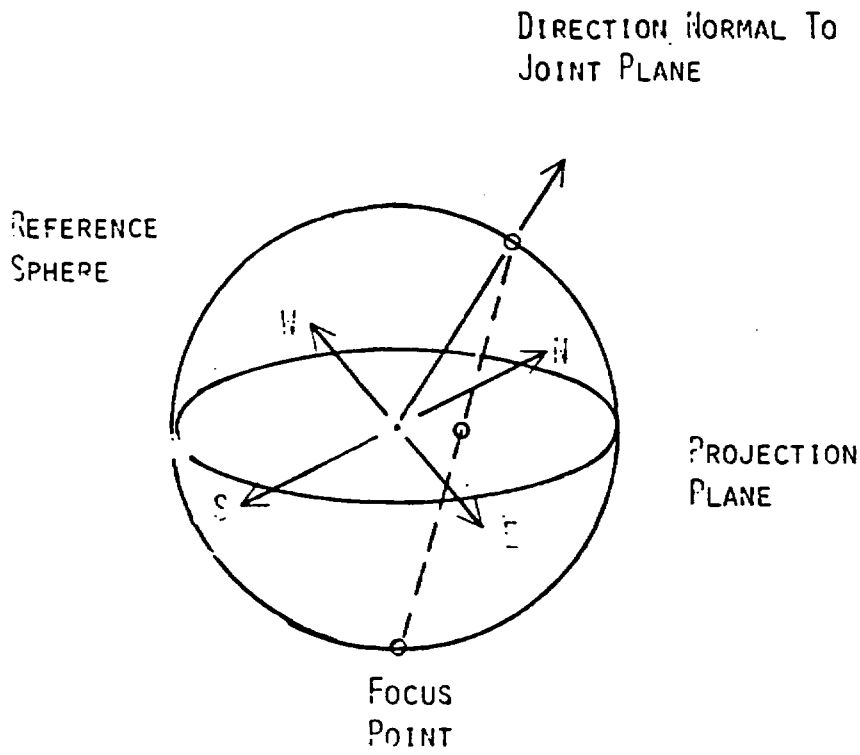

Fig. 6 Stereographic Projection Of Joint Orientation Data Onto A Plane.

techniques for calculating preferred direction and dispersion consisted solely of visual selection from the stereographic projection. Presently, with the aid of scientific computers, a rigorous statistical treatment of orientation data is possible which yields, in addition to the above, correlation among multiple clusters, anisotropic distributions, and goodness-of-fit estimates [30, 31].

Consider the orientation data for a single fracture set which have been plotted on the equal-area stereonet in Fig. 7. Contours of selected orientation densitites are usually drawn to clarify and enhance the pattern. From Arnold [27] and Fisher [28] the probability that an observed orientation lies within the solid angle ϕ, measured from the mean orientation of the pattern, is given by

$$P(\phi) = \frac{1-e^{k(\cos\phi-1)}}{1-e^{k}} \quad . \tag{26}$$

This is the hemispherical normal distribution function, and is applied to circular clusters with a central value of high concentration and which monotonically and isotropically decrease to zero or a uniform background. It is rotationally symmetric about the central value. Since data on the projection plane are plotted for only the upper hemisphere of the reference sphere, the solid angle Φ takes on values $0 \leq \Phi \leq \frac{\pi}{2}$. The value k describes the scatter of

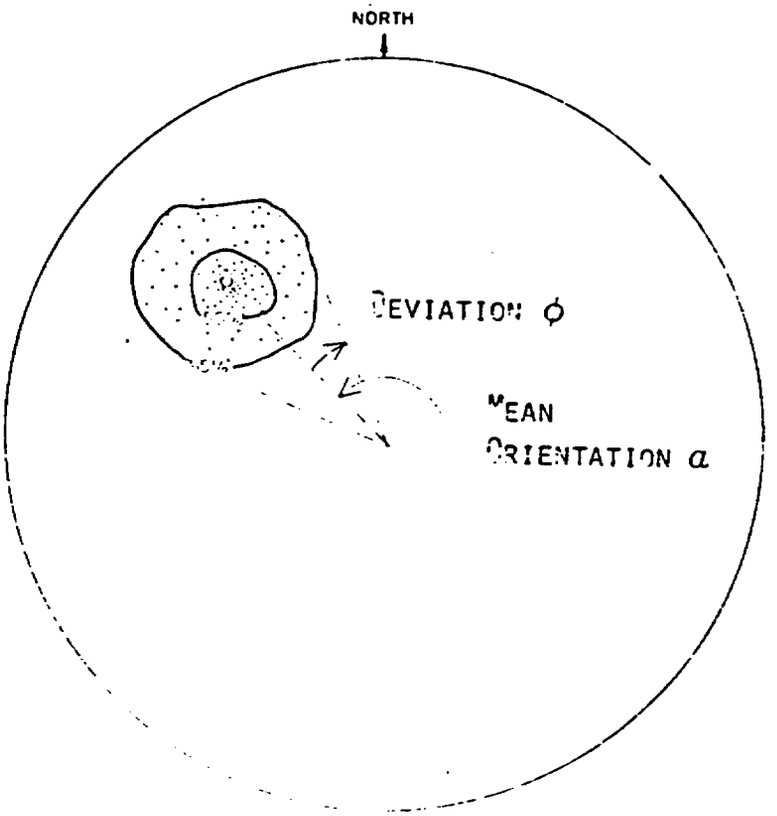

FIG. 7 PROBABILITY ON THE SPHERE FOR JOINT ORIENTATION FIELD DATA. TAKEN FROM GOODMAN [1]

observations and is called the dispersion coefficient, or dispersivity. If the data points are uniformly dispersed over the projection plane, then k = 0 and the fracture plane orientations are randomly distributed. If all data points plot as a single point, then k = ∞ and the fracture planes are parallel. Thus, large values of the dispersion coefficient indicate small scatter. Mahtab, et. al, [26], and others show that if the number of observations is large, and k > 6, then Eq. (26) can be written approximately

$$P(\phi) = 1-e^{k(\cos\phi-1)}, \qquad (27)$$

and which is shown plotted in Fig. 8 for various dispersion coefficients. A dispersion coefficient of 10 means that 50% of the joint planes are expected to be orientated within 22° of the mean direction of the joint set. The standard deviation of the probability function is $k^{-1/2}$.

The technique for initializing fracture angles within the context of a finite element computer code is straightforward. Both the mean orientation α of the joint set to be modelled and the dispersivity k are assumed to be known. For each finite element integration point at which a fracture plane exists, a random number is generated from a uniform distribution defined over the interval (0, 1). This value is assigned to the

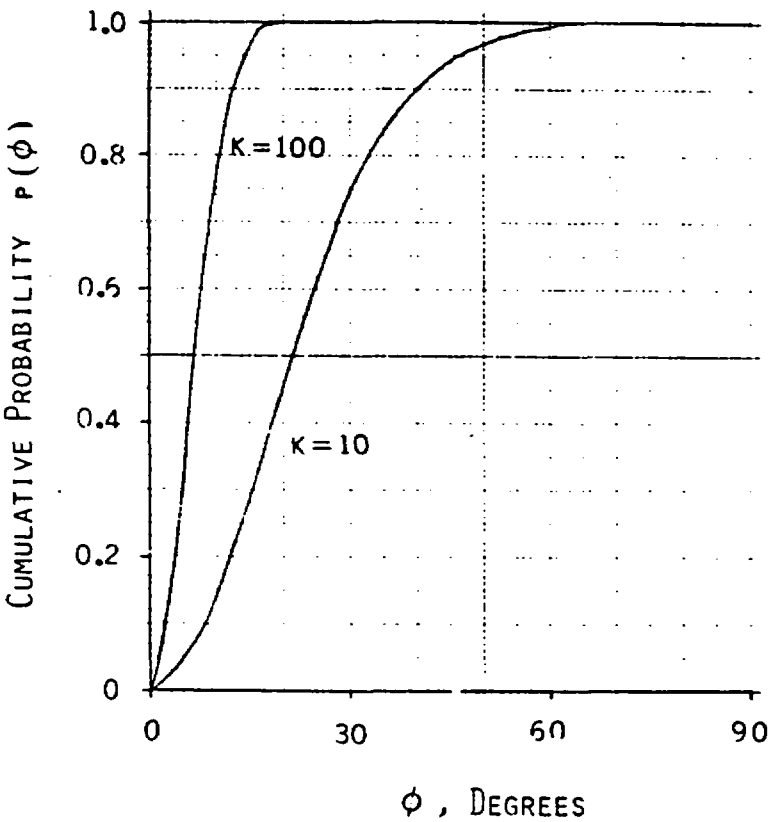

FIG. 8 THE HEMISPHERICAL NORMAL DISTRIBUTION, GIVEN BY

$$P(\phi) = 1 - \exp[K(\cos\phi - 1)],$$

USED TO MODEL JOINT ORIENTATION FIELD DATA.

cummulative probability P (ϕ). The deviation from the mean, ϕ, is then obtained from Eq. (27) with the appropriate dispersion coefficient. Because Φ is actually a solid angle as shown in Fig. 7, an additional step is necessary for two-dimensional models. In this case, the solid angle Φ is projected onto a plane by a direction cosine having the angle $p\pi$, where p is again a random number generated from a uniform distribution defined on the interval (0, 1). Finally, the local fracture angle β is given by

$$\beta = \alpha + \Phi\cos(p\pi) \quad . \tag{28}$$

It can be seen that the population of joint angles selected in this manner will be dispersed according to the original hemispherical normal distribution. If two intersecting fracture sets are to be modelled, the second angle is selected in a similar manner but independent from the first angle, in the sense that the fixed angle between the mean directions of the two joint sets is not maintained locally.

NUMERICAL EXAMPLE: STRESS CONCENTRATION AT AN UNDERGROUND OPENING

The two-dimensional model for a jointed rock mass was programmed for the computer as a discrete, modular package which would be compatible with several structural mechanics

computer codes currently available. The package included both the initialization procedure to quantify the in-situ state of the jointed rock mass to be analyzed, and the stress-strain constitutive relationship. It was first implemented in the ADINA code [26], but only after the program structure was altered by Biffle [32] so that it would accept a constitutive model in modular form. Two new plot programs were developed in order to visually display the kinematics at the joint surfaces. These are simple modifications of the DMESH code [33]. The first, called ANGLE-PLOT, plots the fracture orientation at each finite element integration point. The second, called SLIP-PLOT, plots the present state of the fracture, i.e., whether open, closed, or closed and sliding.

The mechanical behavior of underground nuclear waste repositories is modelled to assess the structural integrity of the underground rooms and the separating pillars during both excavation and subsequent thermal loading. In this example, we consider the excavation problem alone, i.e., the disturbance of the in-situ stress state due to the introduction of an underground opening. A typical configuration for near field "room-and-pillar" calculations is shown in Fig. 9, and a plane strain finite element mesh of the region of interest is shown in Fig. 10. For this example, the extraction ratio is 0.2, the room width is 5m and the room height is 5m. Due to symmetry it

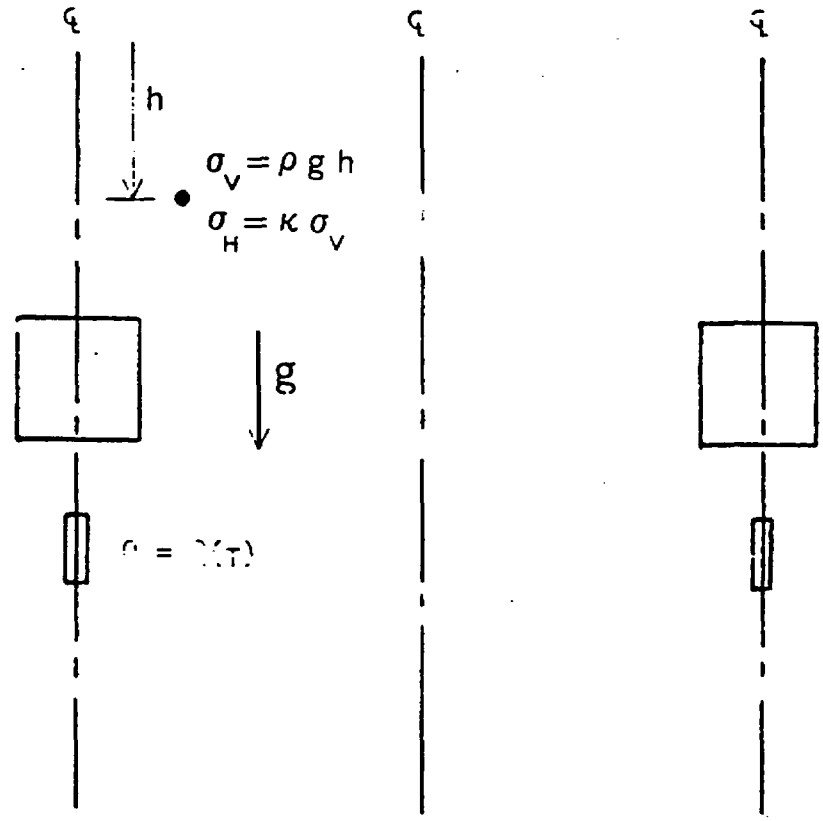

FIG. 9 TWO-DIMENSIONAL GEOMETRY FOR ROOM-AND-PILLAR CALCULATIONS.

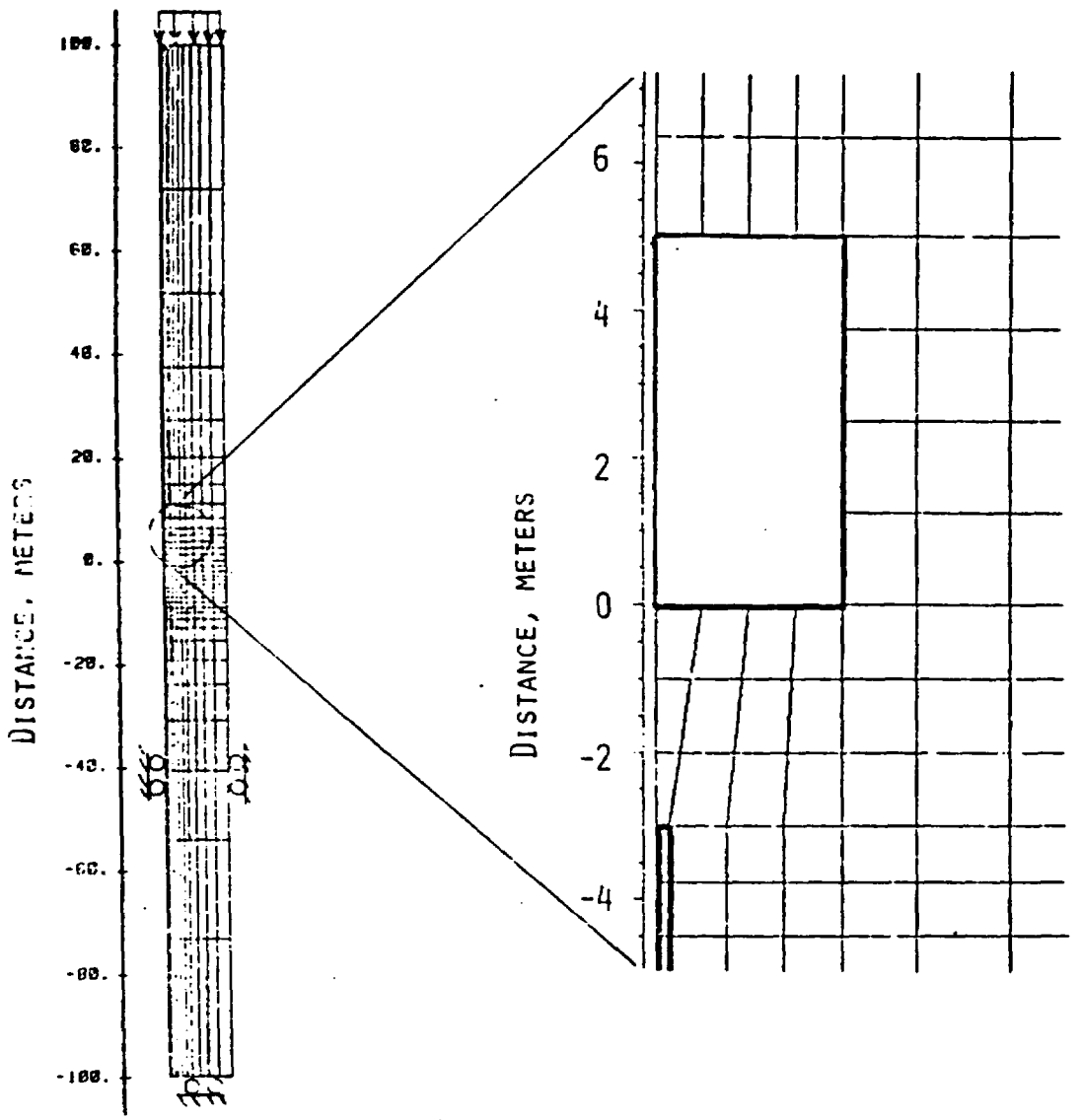

FIG. 10 FINITE ELEMENT MESH FOR PRELIMINARY 2-D MECHANICAL SCOPING STUDIES. THE MESH IS COMPOSED OF 350 4-NODE ISOPARAMETRIC ELEMENTS AND 396 NODE POINTS.

is sufficient that the model extend horizontally from the room centerline to the pillar centerline. The top and bottom boundaries of the mesh are 100m above and below the drift floor, respectively. The drift floor is taken to be 800m below the surface of the earth, and we assume a lithostatic in-situ stress. Given a material density of

$$\rho = 2100 \frac{kg}{m^3}, \tag{29}$$

the initial horizontal and vertical stress components are

$$\sigma_H = \sigma_V = \rho g h, \tag{30}$$

where g is the gravitational constant and h is the distance below the surface of the earth. At the level of the drift floor, a depth of 800m, the lithostatic stress is therefore equal to 16.46 MPa.

For the first calculation the geologic medium was assumed to be isotropic and elastic, having the following material properties:

$$\begin{aligned} E &= 20 \text{ GPa} \\ \nu &= 0.25 \\ G &= 8 \text{ GPa} \end{aligned} \tag{31}$$

A contour plot of the calculated vertical stress component is shown in Fig. 11. It is evident from this plot that a large stress concentration exists at the vertical wall of the drift.

For the second calculation, the medium was considered to be highly fractured by two intersecting joint sets with average orientation of 45° and 135° with respect to the horizontal. This is shown in Fig. 12. Each joint set was assumed to have perfectly parallel fracture planes (dispersion coefficient $k=\infty$). Frictional slippage was governed by a linear Mohr-Coulomb failure envelope defined by two parameters,

$$C_0 = 0 \qquad (32)$$
$$\tan\phi = 0.6 \ .$$

A contour plot of the vertical stress component after excavation is shown in Fig. 13. In contrast to the previous elastic calculation, the stress concentration has moved away from the vertical wall of the drift by a distance approximately equal to one-half the width of the drift. The reason for this "halo" of concentrated compressive stresses surrounding the drift is best illustrated by Fig. 14 in which the stress state at a point on the vertical wall of the drift is plotted on a Mohr diagram. The horizontal stress component σ_H is zero and, if the shear stress on the joint planes is to lie within the prescribed failure envelope, then the vertical stress component

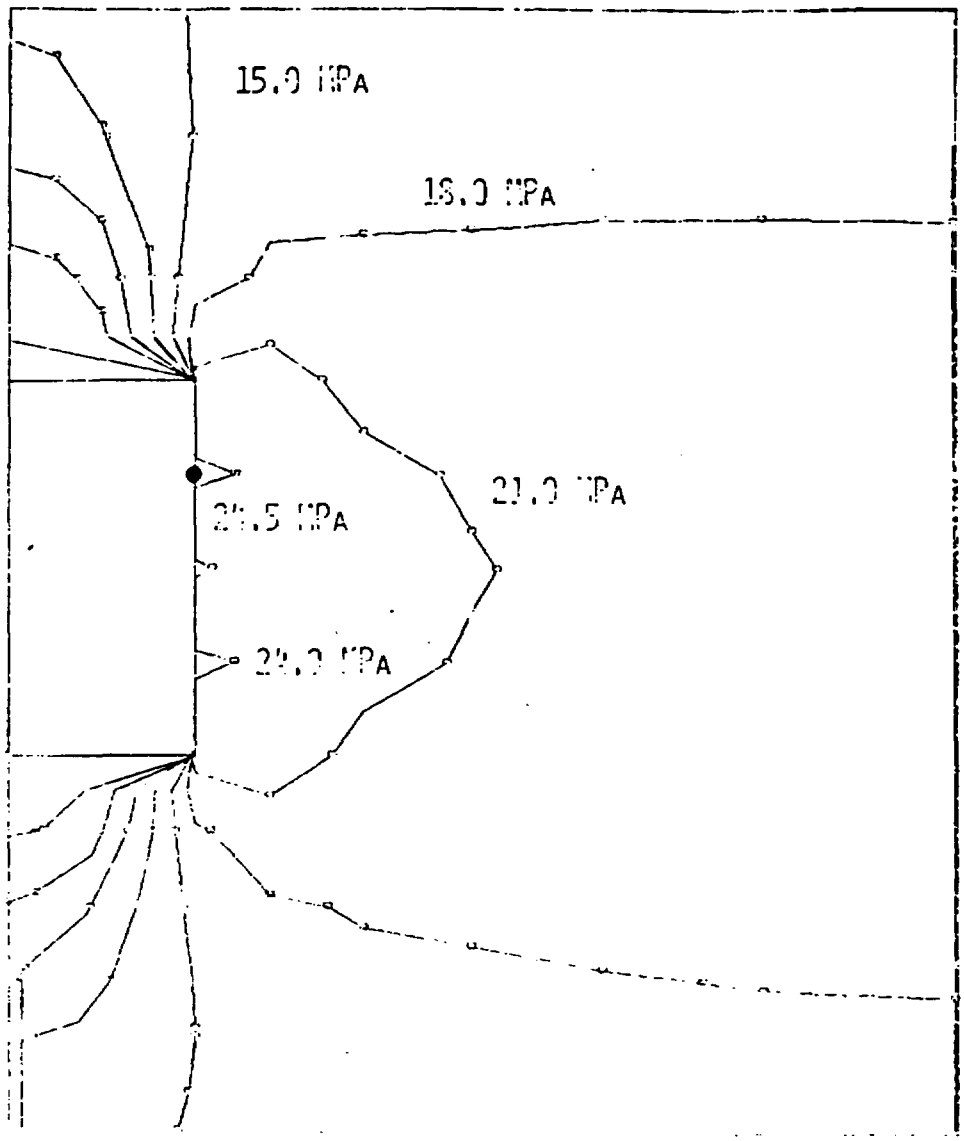

FIG. 11 CONTOURS OF THE VERTICAL STRESS FOR AN UNDERGROUND OPENING IN A MEDIUM WITH ELASTIC MATERIAL PROPERTIES.

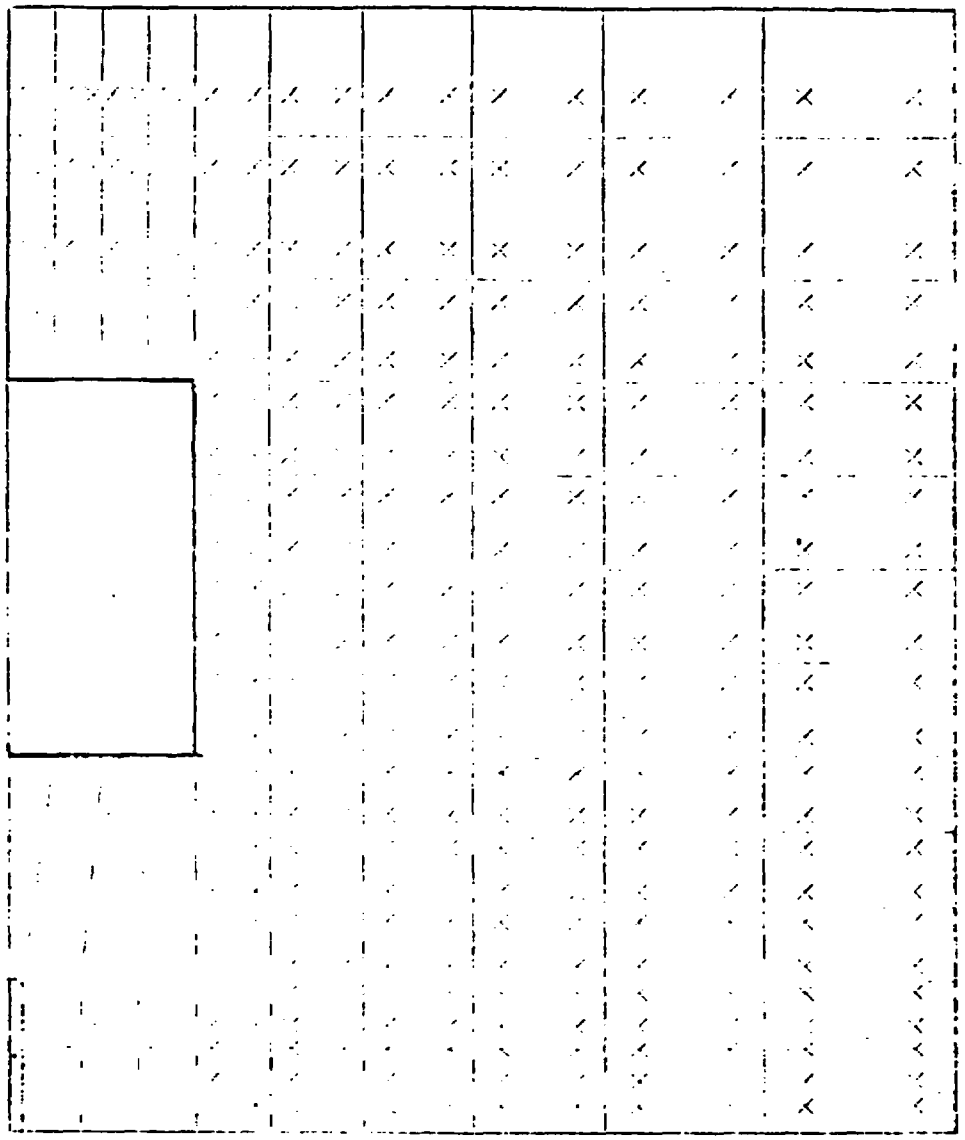

FIG. 12 ORIENTATIONS FOR TWO INTERSECTING JOINT SETS AT 45° AND 135° WITH K=∞ IN A FINITE ELEMENT MODEL.

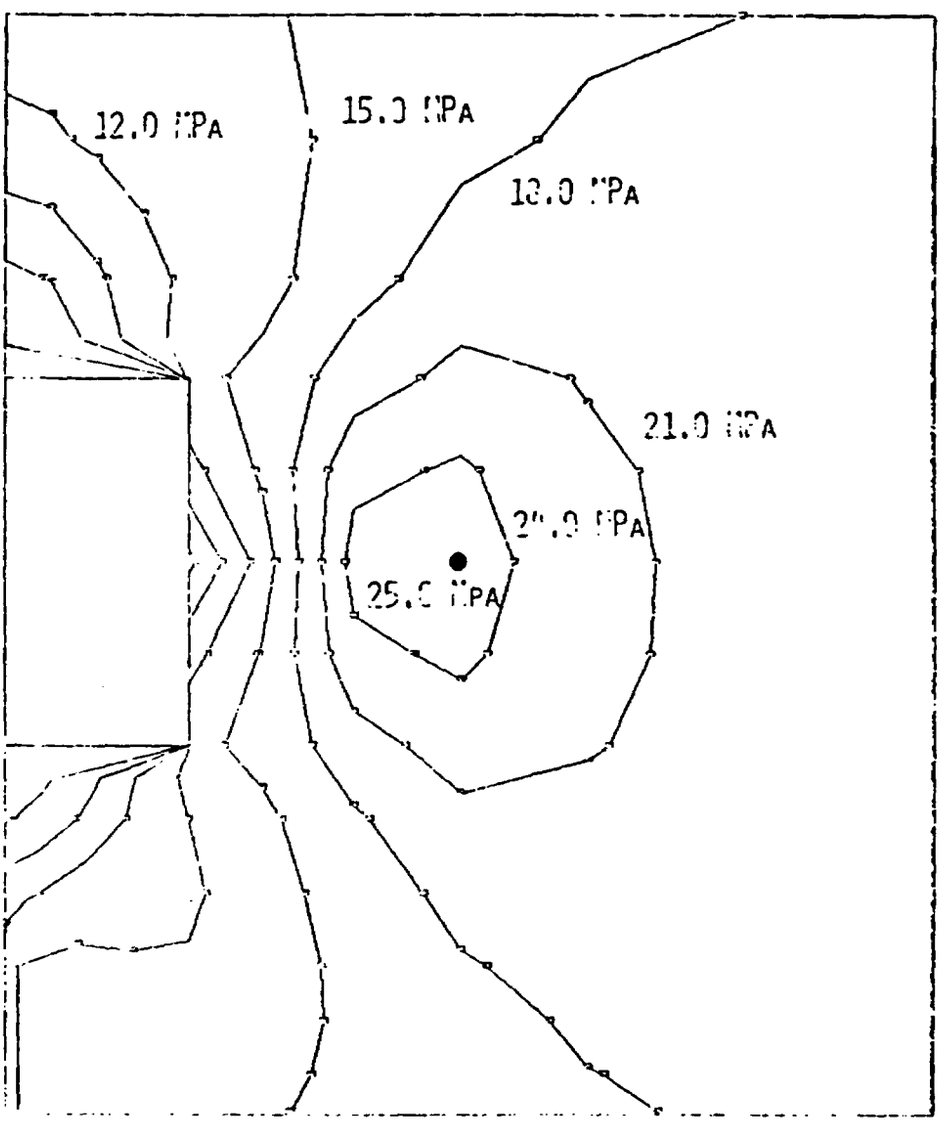

FIG. 13 CONTOURS OF THE VERTICAL STRESS FOR AN UNDERGROUND OPENING IN A MEDIUM WITH TWO INTERSECTING JOINT SETS AT 45° AND 135° WITH $K=\infty$.

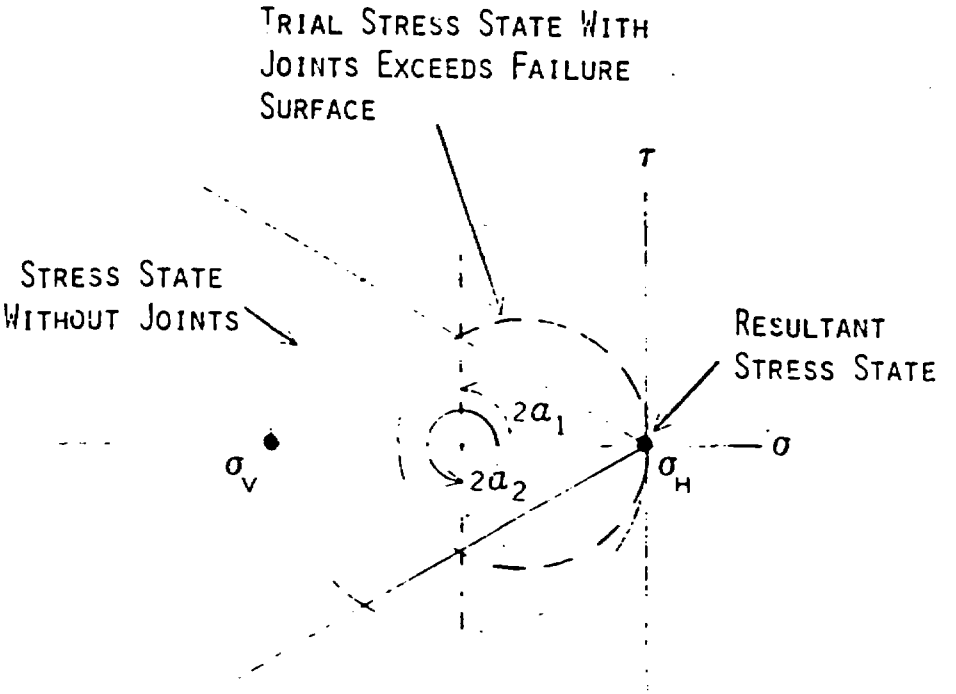

FIG. 1? MOHR'S CIRCLE SHOWING THE ALTERED STRESS STATE AT THE VERTICAL WALL OF THE DRIFT DURING EXCAVATION FOR (45°,135°) INTERSECTING JOINT SYSTEM. FOR THE FAILURE SURFACE SHOWN, THE RESULTANT STRESS STATE IS $\sigma_V = \sigma_H = 0$.

can only be zero. Since the vertical component of stress is zero at the wall of the drift, it must therefore be concentrated somewhere removed from the drift for equilibrium to be maintained. It is also clear from Fig. 14 that this situation would not exist if either the cohesion C_0 were finite, or if the joint sets were orientated such that

$$0 \leqq \alpha_1 \leqq \tan^{-1}\mu \tag{33}$$

and

$$(\pi - \tan^{-1}\mu) \leqq \alpha_2 \leqq \pi \quad .$$

Locations where frictional slippage along joint planes has occurred are shown in Fig. 15. All fractures were assumed to be initially closed and none have opened due to excavation.

In the third and final calculation the joint orientations were taken to be highly dispersed (k = 10), yet the fracture spacing remained infinitesimal. The initial joint angles are shown in Fig. 16, and the calculated vertical stresses are shown in Fig. 17. Again, the stress concentration is removed from the drift wall. The stress gradients around the drift, however, are much less severe because, due to the variable joint orientations, the vertical stresses are not necessarily zero at the wall of the drift. The results of this calculation clearly differ from both those based on the elastic assumption

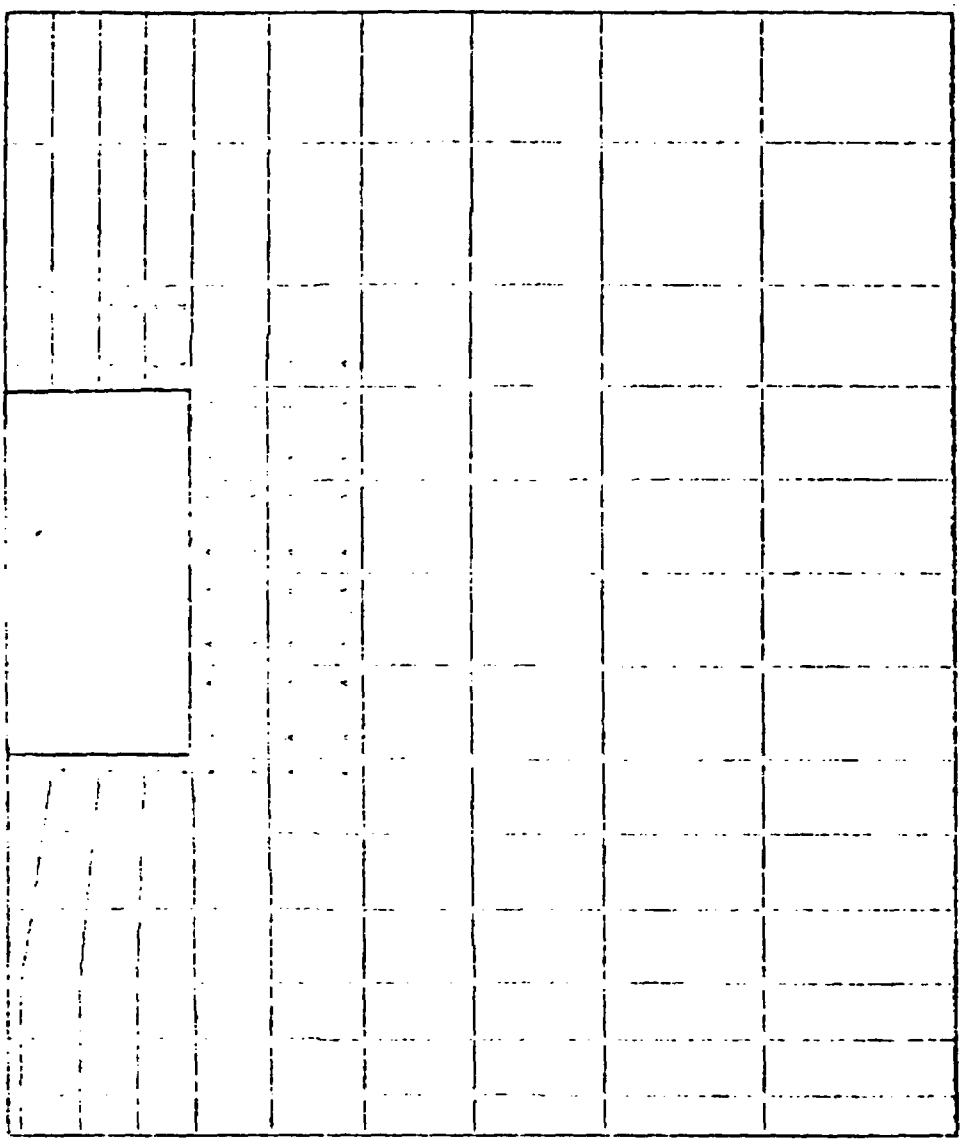

FIG. 15 LOCATIONS OF CALCULATED FRICTIONAL SLIPPAGE ON EITHER JOINT SET AT 45° AND 135° WITH $K=\infty$ FOR AN UNDERGROUND OPENING.

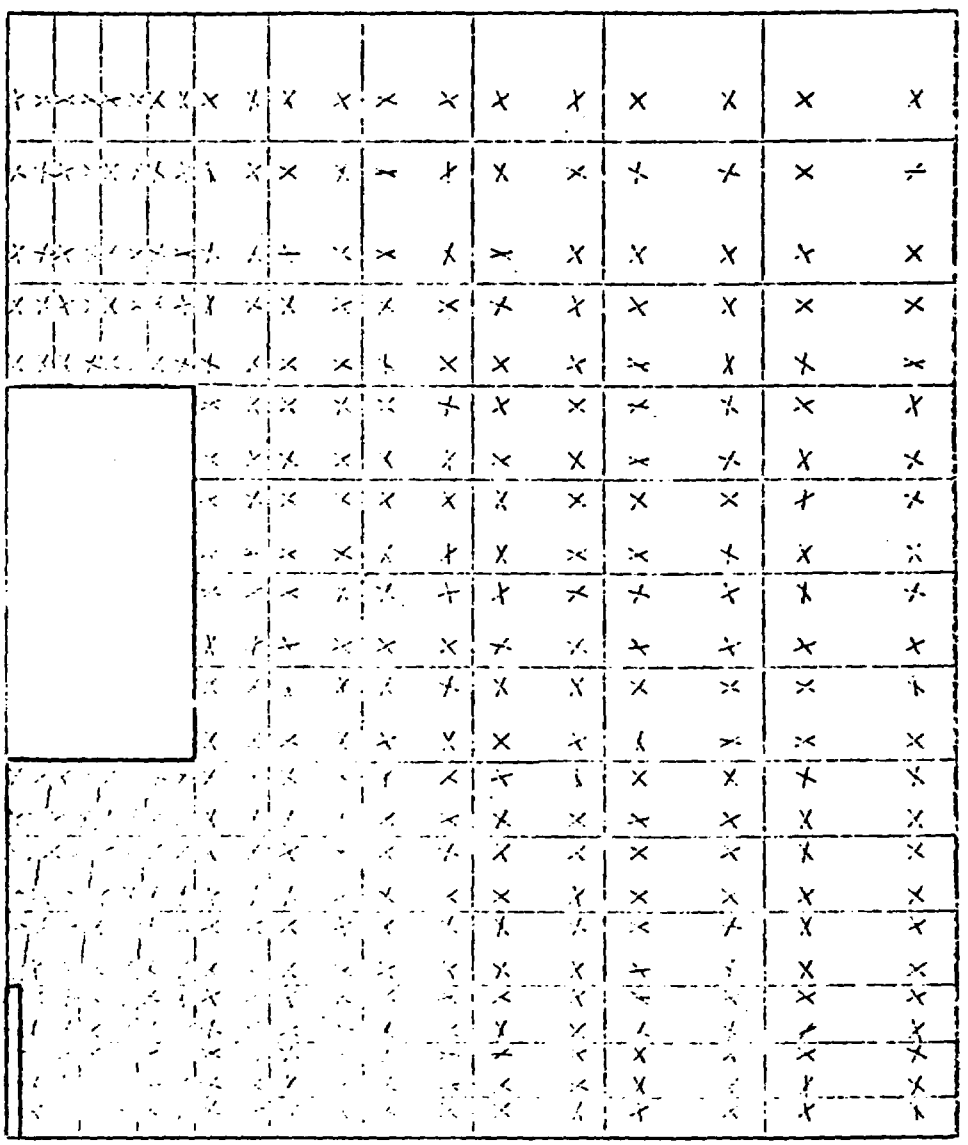

FIG. 16 POSSIBLE ORIENTATIONS FOR TWO INTERSECTING JOINT SETS AT 45° AND 135° WITH K= 10 IN A FINITE ELEMENT MODEL.

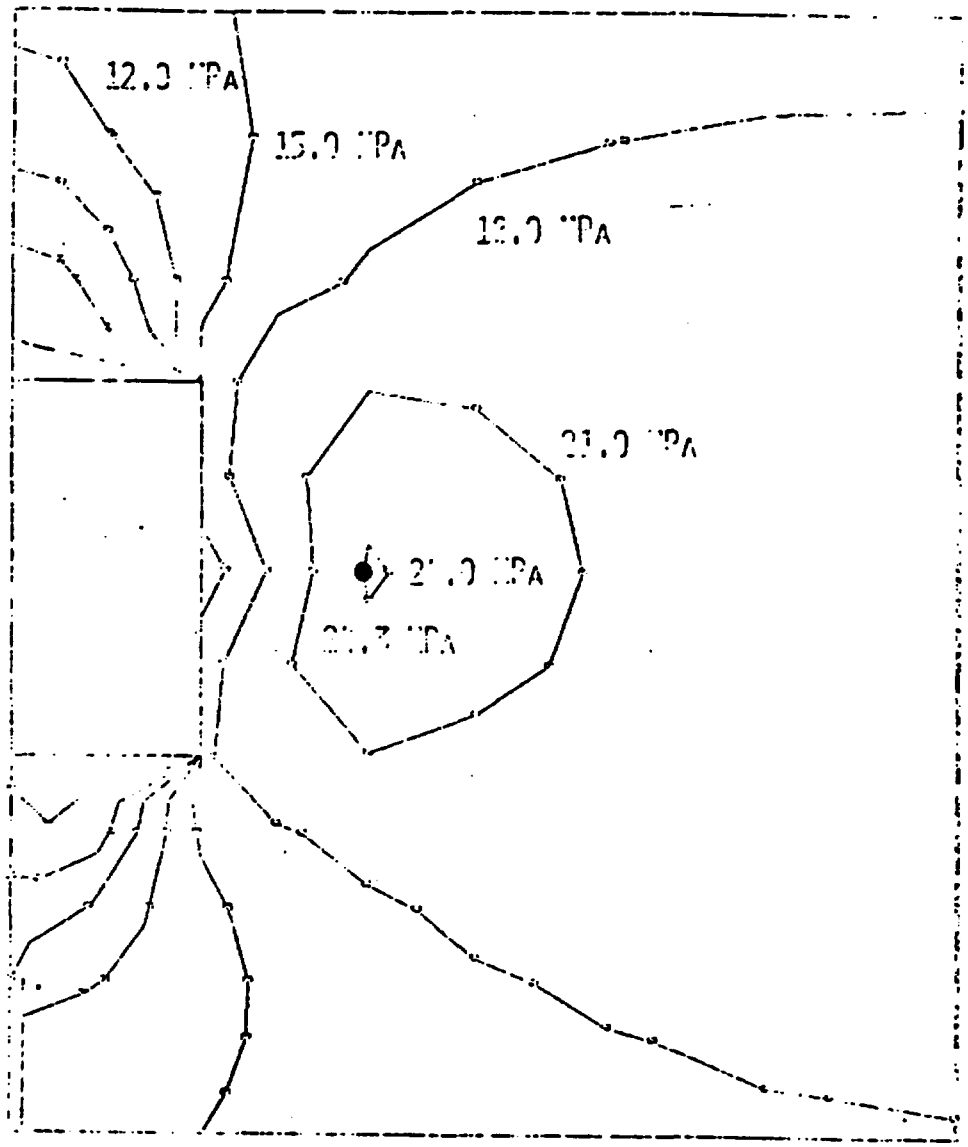

FIG. 17 CONTOURS OF THE VERTICAL STRESS FOR AN UNDERGROUND OPENING IN A MEDIUM WITH TWO INTERSECTING JOINT SETS AT 45° AND 135° WITH K=10.

and those based on the parallel plane assumption. Frictional slippage along the first joint set is shown in Fig. 18, and that along the second joint set in Fig. 19. Several initially closed fractures in the second joint set have opened due to excavation. It must be remembered that, because of the statistical nature of the local joint orientations, these results are not mathematically unique. Additional computer calculations using the same population distribution for joint angles would surely yield different results locally, although the global response may be the same. This is caused by the uncertainty in field measurement data.

FUTURE WORK

The constitutive equations presented in this paper are only the first step toward modelling the behavior of a jointed rock mass. As such, only the basic mechanics of joint slippage, and the corresponding finite element implementation, were emphasized. The future work is divided into two parts: extension of the mechanical model, and coupling with thermal and fluid flow models.

With regard to extension of the mechanical model, it is imperative that a consistent methodology be defined for modelling variable joint spacing which is independent of finite element mesh size. An additional consideration in this effort

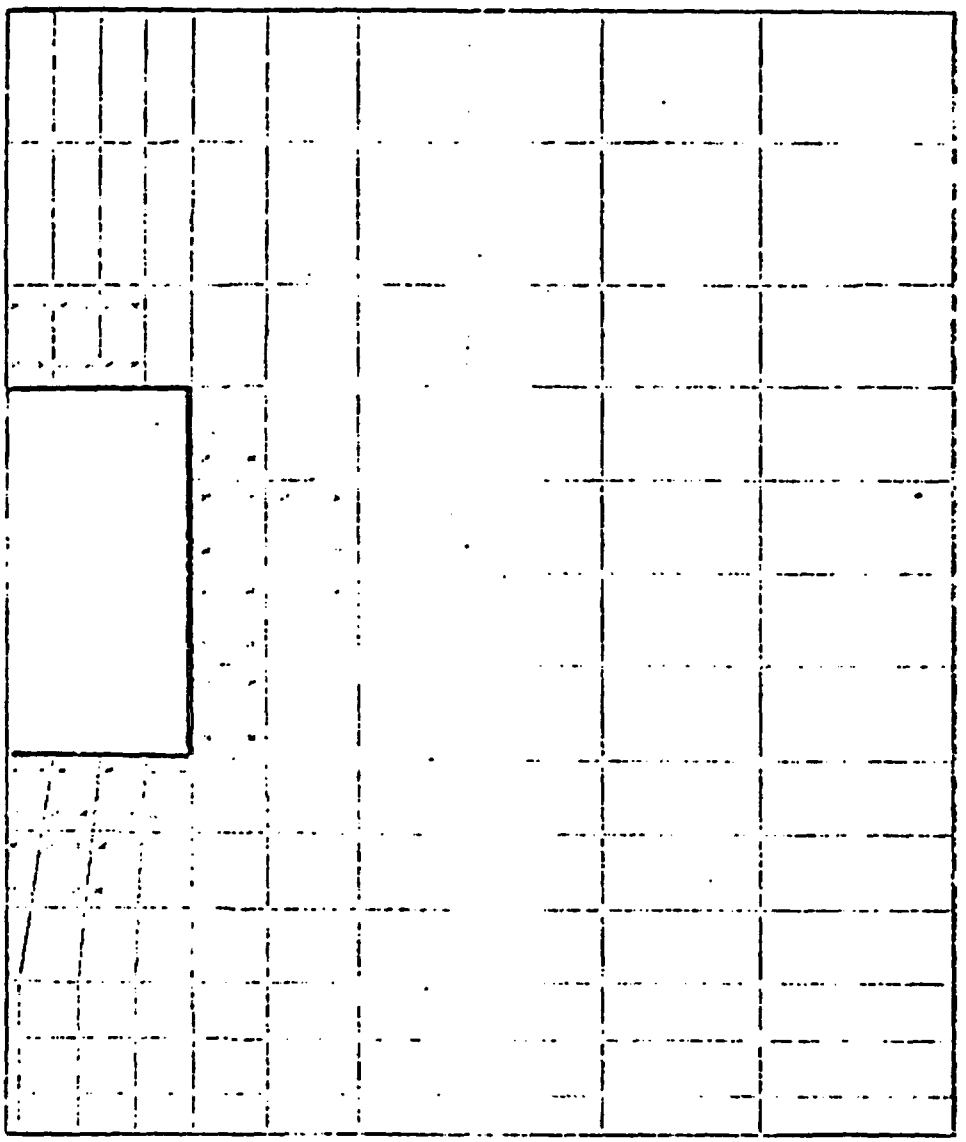

FIG. 13 LOCATIONS OF CALCULATED FRICTIONAL SLIPPAGE ON JOINT SET AT 5° WITH K=10 FOR AN UNDERGROUND OPENING.

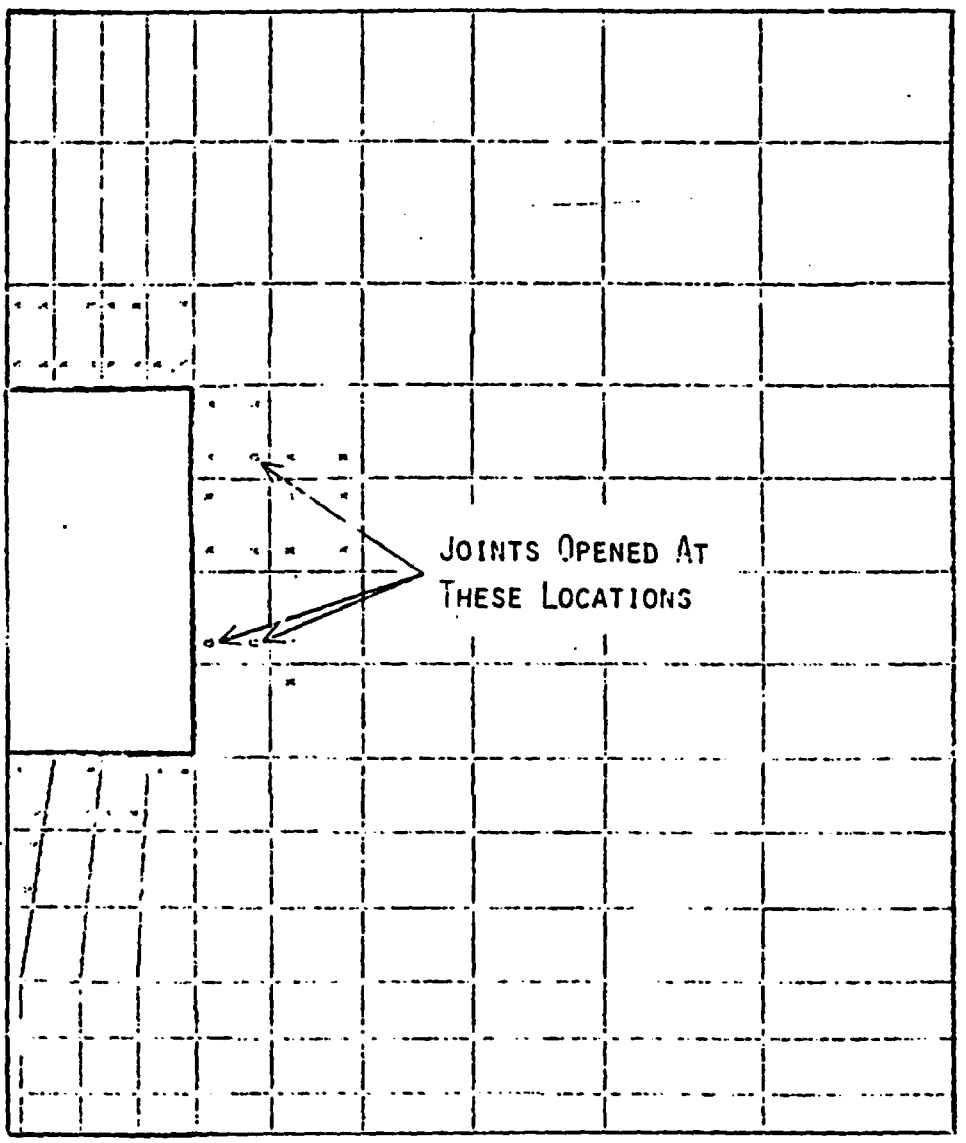

FIG. 19 LOCATIONS OF CALCULATED FRICTIONAL SLIPPAGE ON JOINT SET AT 135° WITH K=10 FOR AN UNDERGROUND OPENING

is potential cross-correlation between joint orientation and joint spacing. Also planned are investigations of post-slippage dilatancy, shear lock-up due to corner interactions, and crack initiation in the intact rock. In the near future, increasingly detailed analyses will be required, particularly in the area of waste repository calculations, and this will dictate a three-dimensional version of the jointed rock model. It appears that joint planes in three-dimensions can be readily prescribed and modelled by explicit modification of the constitutive equations, but the computer run times for these highly nonlinear problems is presently unknown. Present run times on a CDC7600 computer for similar three-dimensional problems with geological materials varies from 700 to 3000 seconds per load step depending upon the degree of nonlinearity [34]. The run time for a three-dimensional version of the jointed rock model is not expected to be any less. Since many load steps are required to trace the thermal history of a nuclear waste repository, it is possible that future calculations may be limited by present computers.

The model presented in this paper could serve in future work as the basis for studying the interactions among mechanical deformations, heat transfer, and fluid flow in a regularly jointed medium. The coupling mechanism is the orientation and gap opening of the joint. In particular, the permeability tensor for fluid flow becomes anisotropic in the

vicinity of a fracture, and highly dependent on gap opening for flow parallel to the fracture. A similar statement can be made with regard to the conductivity tensor for heat transfer. If three-dimensional mechanical calculations are potentially limited by present computer capability, then three-dimensional coupled calculations are surely limited.

REFERENCES

1. R. E. Goodman, Methods of Geological Engineering In Discontinuous Rock, West Pub. Co., 1976.

2. N. J. Price, Fault and Joint Development in Brittle and Semi-Brittle Rock, Pergamon Press, 1966.

3. International Society for Rock Mechanics Commission on Standardization of Laboratory and Field Tests, Suggested Methods for the Quantitative Description of Discontinuities in Rock Masses, Int. J. Rock Mech. Min. Sci. and Geomech. Abstr., Vol. 15, p. 319, 1978.

4. McVey, D. F., A. R. Lappin, and R. K. Thomas, Test Results and Supporting Analysis of a Near-Surface Heater Experiment in the Eleana Argillite, pp. 93-1'0 in Proceedings of the NEA Workshop on the Use of Argillaceous Materials for the Isolation of Radioactive Wastes, held Paris, France, Sept. 10-12, 1979. Published by NEA/OECD, Paris, France, 1980.

5. S. F. Reyes and D. U. Deere, Elastic-Plastic Analysis of Underground Openings by the Finite Element Method, Proc. First Cong. ISRM, Lisbon, Vol. 2, p. 477, 1966.

6. W. G. Pariseau, B. Voight and H. D. Dahl, Finite Element Analysis of Elastic-Plastic Problems in the Mechanics of Geologic Media, Proc Second Cong. ISRM, Belgrade, Vol. 2, paper 3-45, 1970.

7. O. C. Zienkiewicz, S. Valliappan and I. P. King, Stress Analysis of Rock as a No-Tension Material, Geotechnique, Vol. 18, p. 56, 1968.

8. R. E. Goodman, R. L. Taylor and T. L. Brekke, A Model for the Mechanics of Jointed Rock, J. SMFD ASCE, Vol. 94, p. 637, 1968.

9. J. Ghaboussi, E. L. Wilson and J. Isenberg, Finite Element for Rock Joints and Interfaces, J. SMFD ASCE, Vol. 99, p. 833, 1973.

10. W. J. Roberds, Numerical Modelling of Rock Joints, Proc. Twentieth Symp. Rock Mech. ,Austin, Texas, June, 1979, p. 233.

11. J. D. Dixon and M. A. Mahtab, A Method for Computing Stabilization Pressures for Excavations In Incompetent Rock, USB Mines RI 8128, 1976.

12. P. Cundall, A Computer Model for Simulating Progressive Large Scale Movements in Blocky Rock Systems, Proc. Int. Symp. on Rock Fracture, Nancy, Paper 2-8, 1971.

13. B. Singh, Continuum Characterization of Jointed Rock Masses, Part I - The Constitutive Equations, Int. J. Rock Mech. Min. Sci. and Geomech. Abstr, Vol. 10, p. 311, 1973.

14. L. W. Morland, Continuum Model of Regularly Jointed Mediums, J. Geophysical Research, Vol. 79, No. 2, p. 357, 1974.

15. O. C. Zienkiewicz and G. N. Pande, Time-Dependent Multilaminate Model of Rocks - A Numerical Study of Deformation and Failure of Rock Masses, Int. J. For Numerical and Analytical Methods in Geomechanics, Vol. 1, p. 219, 1977.

16. Radioactive Waste Repository Study, Topical Report 11 - Room Stability, Acres Consulting Services Limited, Niagara Falls, Ontario, and Atomic Energy of Canada Limited, 1977.

17. D. M. Cruden, Describing the Size of Discontinuities, Int. J. Rock Mech. Min Sci. and Geomech. Abstr., Vol. 14, p. 133, 1977.

18. D. T. Snow, The Frequency and Aperatures of Fractures in Rock, Int. J. Rock Mech. Min. Sci., Vol. 7, p. 23, 1970.

19. S. D. Priest and J. A. Hudson, Discontinuity Spacings in Rock, Int. J. Rock Mech. Min. Sci. and Geomech. Abstr., Vol. 13, p. 135, 1976.

20. P. E. Long, Characterization and Recognition of Intraflow Structures, Grande Ronde Basalt, RHO-BWI-LD-10, Rockwell International, Hanford Operations, Sept., 1978.

21. R. Thorpe, Characterization of Discontinuities in the Stripa Granite Time-Scale Heater Experiment, LBL-7083, SAC-20, UC-70, Lawrence Berkeley Laboratory, July, 1979.

22. R. L. Johnson and R. T. Henderson, FASOR - A Finite Element Program for Failure Analysis of Solids of Revolution, CE-37(72) SL - 196-1, University of New Mexico, Bureau of Engineering Research, 1972.

23. R. M. Jones, Mechanics of Composite Materials, Scripta Book Co., 1975.

24. K. J. Bathe and S. Ramaswamy, On Three-Dimensional Finite Element Analysis of Concrete and Rock Structures, J. Nuclear Eng. and Design, Vol. 52, p. 385, 1979.

25. R. K. Thomas and G. R. Hadley, Numerical Computation of Thermal and Pressure Stresses in Low Tensile Strength Geologic Media, SNL Tech. Memo, Apr. 20, 1979.

26. K. J. Bathe, ADINA - A Finite Element Code for Automatic Dynamic Incremental Nonlinear Analysis, MIT Report 82448-1, December, 1978.

27. K. J. Arnold, On Spherical Probability Distributions, PhD Thesis, MIT, 1941.

28. R. A. Fisher, Dispersion on a Sphere, Proc. Roy. Soc., London, Ser. A, Vol. 217, May, p. 295, 1953.

29. G. S. Watson, The Statistics of Orientation Data, J. Geol., Vol. 74, No. 5, p. 786, 1966.

30. H. J. Pincus, The Analysis of Aggregates of Orientation Data in the Earth Sciences, J. of Geol. Vol. 61, p. 482, 1953.

31. M. A. Mahtab, D. D. Bolstad, J. R. Alldridge, and R. J. Shanley, Analysis of Fracture Orientations for Input to Structural Models of Discontinuous Rock, U.S.B. Mines RI 7669, 1972.

32. Modifications to ADINA by J. H. Biffle, Sandia National Laboratories, Albuquerque, NM, have not been published.

33. Z. E. Beisinger and S. E. Benzley, Structural Mechanics Computer Plotting Handbook, SAND75-0038, Sandia National Laboratories, Albuquerque, NM, 1975.

34. R. K. Thomas, A. R. Lappin and M. H. Gubbels, Three-Dimensional Thermal and Mechanical Scoping Calculations for Underground Nuclear Waste Disposal in Shales, SAND80-2507, in preparation.